EUROfusion

EUROFUSION WPMST1–PR(15)04

B. Geiger et al.

Fast-ion Transport and Neutral Beam Current Drive in ASDEX Upgrade

Preprint of Paper to be submitted for publication in
Nuclear Fusion

This work has been carried out within the framework of the EUROfusion Consortium and has received funding from the Euratom research and training programme 2014-2018 under grant agreement No 633053. The views and opinions expressed herein do not necessarily reflect those of the European Commission.

Fast-ion transport and neutral beam current drive in ASDEX Upgrade

B Geiger[1], M Weiland[1], A S Jacobsen[2], D Rittich[1], R Dux[1], C Hopf[1], S K Nielsen[2], M Reich[1], M Salewski[2], P A Schneider[1], G Tardini[1], the ASDEX Upgrade team[1]

[1] Max-Planck-Institute for Plasma Physics, Boltzmannstr. 2, 85748 Garching, Germany

[2] Technical University of Denmark, Department of Physics, Dk-2800 Kgs. Lyngby, Denmark

PACS numbers: 52.55.Fa, 52.50.Gj, 52.55.Tn, 52.55.Wq

Abstract.

The confinement of suprathermal fast ions generated by neutral beams was investigated in the ASDEX Upgrade tokamak. Strong sawtooth-induced internal redistribution of co-rotating fast-ions is measured and very well described by the Kadomtsev model. Reconstructions of the 2D fast-ion velocity distribution function by a tomographic inversion of multiple FIDA spectra in the plasma center indicate strong sawtooth-induced ejection of mainly co-rotating fast ions and a weaker redistribution of fast ions with smaller pitches. The fast-ion current drive efficiency has been studied in discharges with on- and off-axis NBI. During radial on-axis NBI the fast-ion and current profiles are peaked in the center, whereas they are both shifted outwards during tangential off-axis NBI. Comparisons with neoclassical predictions from TRANSP are in rough agreement with the observation for on-axis NBI whereas a stronger current drive and more peaked profiles are expected but not observed for off-axis NBI. The discrepancy can possibly be explained by weak MHD activity or turbulence-induced fast-ion transport.

1. Introduction

In present day fusion devices fast ions are mainly generated by neutral beam injection (NBI). They heat plasmas through collisions with electrons and ions and, if injected with a sufficiently parallel velocity component, their associated current drive can be used to reach non-inductive conditions or to tailor the plasma current profile [1]. Well confined fast ions are, hence, essential to obtain good heating and current drive performances. In addition, detailed understanding of the fast-ion transport mechanisms is needed in view of future fusion devices, not only to guarantee good performance, but also to ensure the safety of the machine: fast helium ions will be produced in fusion reactions that could, if poorly confined, damage the first wall [2]. In toroidally axisymmetric devices such as tokamaks, the fast-ion transport induced by collisions and orbit effects, i.e. the neoclassical transport, is relatively small. However, enhanced fast-ion transport, caused by large- and small-scale instabilities (anomalous transport), could reduce the fast-ion confinement and must therefore be investigated. In particular, core localized MHD modes must be studied in detail because they spatially overlap with the fast-ion distribution functions which are typically peaked on-axis. One of the most severe types of core-perturbation in tokamak plasmas is induced by sawtooth crashes [3, 4], which are caused by the fast reconnection of a mode with toroidal and poloidal mode numbers of one (n=1 and m=1). They appear periodically in the plasma center when the safety factor, q, is below one and cause a fast crash of the central pressure, followed by a recovery phase. The crashes strongly redistribute fast ions, as reported from D-T experiments at JET [5] and TFTR [6] and from Deuterium plasmas at DIII-D [7], TEXTOR [8], MAST [9] and ASDEX Upgrade [10]. Two mechanisms are in part responsible for the strong redistribution. These are **E**x**B** drift effects and the motion of the fast particles along the evolving magnetic field lines. The details of these mechanisms are, however, not yet clear and need to be investigated in detail.

Of special interest is also the characterization of the off-axis Neutral Beam Current Drive (NBCD) efficiency which is motivated by somewhat contradicting results in the past. On the one hand, previous experiments showed that the evolution of the current profile did not follow neoclassical predictions when replacing on-axis NBI with off-axis NBI. In particular, the effect of off-axis NBCD on measurements of the current profile by a Motional Stark Effect diagnostic (MSE) was weaker than expected by theory [11, 12]. On the other hand, measured radial fast-ion profiles, which are expected to be linked to the beam driven current, exhibited good agreement with neoclassical predictions [13, 14].

This important aspect, as well as the fast-ion redistribution due to sawtooth crashes, has now been revisited in ASDEX Upgrade, motivated by new measurement capabilities. In particular, a fast-ion D-alpha (FIDA[15]) spectroscopy diagnostic is now available that measures radial profiles of co-rotating fast-ions and allows measurements of central 2D fast-ion velocity distribution functions by a tomographic inversion in velocity space.

This paper is structured as follows. In section II, the effect of sawtooth crashes on the fast ions is discussed. Measured neutron rates and radial FIDA profiles of co-rotating ions are compared with theoretical predictions and the central fast-ion velocity space is analyzed using tomographic inversions. A study of off-axis fast-ion populations and the associated NBI current drive is presented in section III. Radial fast-ion profiles and MSE measurements are compared with theoretical predictions. Finally, a short summary and conclusion are given.

2. Sawtooth-induced fast-ion transport

In the 2014 experimental campaign of ASDEX Upgrade [16], experiments were performed with 1 MA of plasma current, a toroidal magnetic field of -2.6 T and 2.5 MW of heating power from one radially injecting on-axis NBI source (NBI Q3) with 60 keV maximum injection energy. The discharges feature low densities ($\approx 4 \times 10^{19}/\mathrm{m}^3$) and high ion temperatures (up to 6 keV) and exhibit strong sawtooth activity, indicated by periodic drops of the central electron temperature, ion temperature and rotation. The effect of the crashes on the fast ions can be seen in figure 1a which illustrates the measured count rate of neutrons, mainly produced by fusion reactions between fast ions and the background plasma. It should be noted that the experimental neutron rate in arbitrary units has been measured by a novel neutron spectrometer [17] that has a very good signal to noise ratio when integrating the measurement in energy but does not provide absolute fluxes. Clearly, the neutron rate decreases periodically with every sawtooth crash, explained by an outwards fast-ion redistribution to a colder plasma region where fast ions are slowed down more quickly. The same behavior can be seen in the predicted neutron rates from TRANSP [18] that are plotted in red. TRANSP uses a Monte Carlo approach to simulate fast ions and needs to be supplied with the evolution of the kinetic profiles, information on the heating sources and on the separatrix position. The code models the effect of sawtooth crashes on the fast ions by applying the Kadomtsev model [19], which assumes full reconnection of the helical magnetic field during sawtooth crashes and redistributes fast particles according to the evolving field

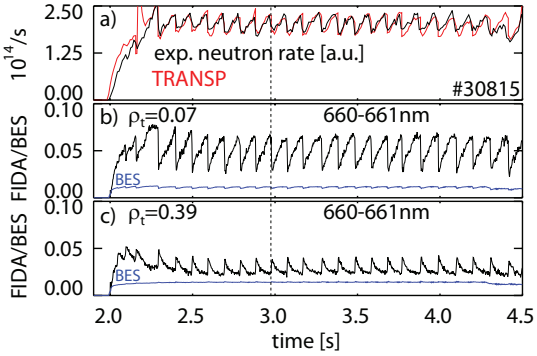

Figure 1. a) Measured neutron rate in arbitrary units, scaled to roughly match the prediction from TRANSP (Kadomtsev model) given in red. b) Temporal evolution of the measured FIDA/BES ratio at $\rho_t = 0.07$ showing a clear reduction of the fast-ion density when sawteeth appear. c) FIDA/BES ratio measured at $\rho_t = 0.39$, indicating an increased fast-ion density after sawtooth crashes outside the sawtooth inversion radius. In blue, the evolution of the beam emission is given in 2×10^{19}photons/s/sr/m^2 which has been used to normalize the FIDA data.

lines. The TRANSP predicted relative change of the neutron rate in figure 1a agrees very well with the relative change in the experimental data showing that the Kadomtsev model well describes the sawtooth-induced fast-ion redistribution.

This is further supported by measurements of the FIDA diagnostic [20] which analyzes the Doppler-shifted Balmer alpha radiation, emitted by fast ions after charge exchange reactions along a neutral beam path. The measured spectral intensities of the FIDA radiation (example spectra can be seen in figure 3) contain information on the fast-ion density and the measured Doppler shifts yield information on the fast-ion velocity distribution. In figures 1b and 1c we show integrated red-shifted FIDA radiation between 660 and 661 nm as a function of time at two radial positions. The data has been measured using toroidal lines of sight (LOS) with a temporal resolution of 2.5 ms and yields information on co-rotating fast-ions with energies above 30 keV (see [14]). In order to take the attenuation of the neutral beam into account and to be independent of the intensity calibration, the measured FIDA radiation has been normalized to the simultaneously measured beam emission (BES) that is also present in the measured spectra. The evolution of the beam emission is plotted in blue in figures 1b and 1c. This contribution changes only weakly when sawtooth crashes appear, which indicates that the probability of fast-ions to undergo change exchange reactions and to emit FIDA radiation is not significantly modified. The strong drops of the central FIDA/BES ratio (figure 1b) and the increased signal outside the q=1 surface (figure 1c) can, consequently,

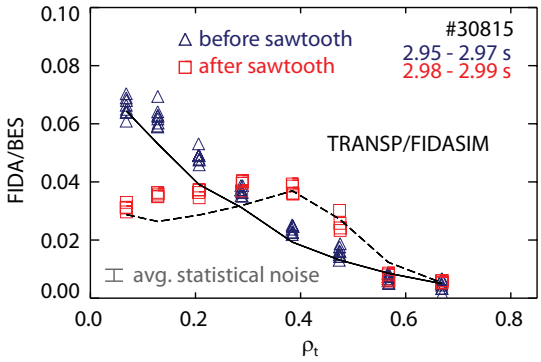

Figure 2. Radial FIDA/BES profiles ($660 - 661$ nm) acquired with a time resolution of 2.5 ms before (blue) and after (red) a sawtooth crash at ≈ 3 s. In black, synthetic profiles from TRANSP/FIDASIM are given. The error-bar plotted in the lower left part of the figure illustrates the average statistical uncertainties of the FIDA measurement.

be attributed to a radial fast-ion redistribution.

Radial profiles of the fast ions are obtained from an array of LOS that cross the path of NBI at different positions. Figure 2 shows radial FIDA/BES profiles before (blue) and after (red) the sawtooth crash at ≈ 3 s as a function of the normalized toroidal flux label, ρ_t. A constant offset has been subtracted from the data to account for passive radiation from the plasma edge. The simulated FIDA/BES profiles, illustrated in black, have been calculated by the post-processor FIDASIM [21] which translates predicted fast-ion distribution functions from TRANSP into synthetic spectra and profiles. The predicted change of the profiles is in good agreement with measurement. This indicates that the sawtooth crashes cause an internal fast-ion redistribution of co-rotating fast-ions that is dominated by the motion of fast particles along the evolving field line, as assumed in the Kadomtsev model.

In order to study the effect of sawtooth crashes on the central fast-ion velocity space distribution of fast ions, a tomographic inversion has been performed that is based on the analysis of FIDA spectra from four different viewing geometries. The method of tomographic inversion has been demonstrated previously [22, 23, 24] and is applied here to measure 2D fast-ion velocity distribution functions as a function of energy and pitch (pitch $= v_{||}/v_{tot}$ where $v_{||}$ is the fast-ion velocity anti-parallel to the magnetic field and v_{tot} is the total fast-ion velocity).

Coherently averaged spectra just before and just after sawtooth crashes are plotted in figure 3 from which passive radiation has been subtracted (coherent averaging has been used between 2.3 s and 4.5 s in discharge #30815 to reduce the statistical uncertainties of the measurement). The spectra have been simultaneously measured

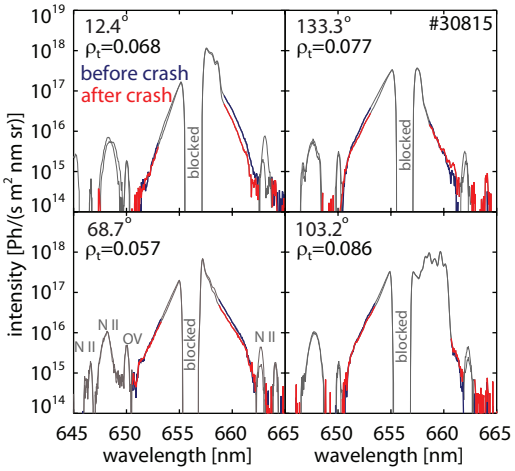

Figure 3. Time coherent averaged spectra containing FIDA radiation before (blue) and after (red) a sawtooth crash from four different viewing geometries on a semi logarithmic scale. The FIDA radiation can mainly be analyzed between 650 and 653 nm and between 659 and 662 nm where it is not superimposed by other spectral contributions, like the cold D-alpha radiation, the beam emission and impurity line emissions. The measured radiation plotted in gray corresponds to the spectral regions that have been excluded from the tomographic reconstruction.

and correspond to LOS that intersect the path of NBI in the plasma center ($\rho_t < 0.09$) with angles to the local magnetic field of 12.4 degrees, 133.3 degrees, 68.7 degrees and 103.2 degrees. Not all wavelength regions can be analyzed by the tomographic inversion because additional spectral components are present, in addition to the FIDA radiation. In particular, the cold D-alpha radiation at 656.1 nm (here blocked by a filter), the beam emission and strong impurity line emissions must be excluded from the analysis. Moreover, we use only FIDA light with Doppler shifts that correspond to fast ions with energies above 10 keV. In consequence, only those parts of the spectra are analyzed that are highlighted in color in figure 3. The radiation in the analyzed wavelength ranges is clearly lower after the averaged sawtooth crash. This indicates a reduction of the central fast-ion density in the different parts of the velocity space that are observed by the four geometries. Each viewing geometry and wavelength range collects FIDA radiation of neutralized fast-ions from different regions in velocity space which is described by FIDA weight functions [25]. The latter are needed as input for the tomographic reconstruction and have been calculated by FIDASIM.

The inferred 2D fast-ion velocity distribution functions just before and just after the coherently averaged sawtooth crash are shown in figures 4a and 4b, respectively. The tomography has been performed on a 15×15 grid in energy and pitch and 32

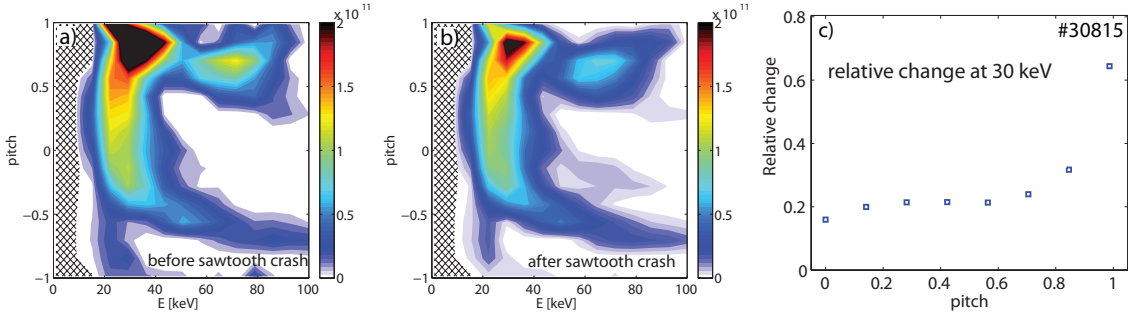

Figure 4. a+b) Reconstructions of the fast-ion velocity-space distribution function in the plasma center (inside q=1) before and after a sawtooth crash in units of [ions/(keVcm^3)]. c) Relative change $(f_{before} - f_{after})/f_{before}$ of the fast-ion density at 30 keV as a function of the pitch value.

levels were used for the singular value decomposition. The influence of the sawtooth crashes on the kinetic profiles and, hence, on the charge exchange and photon emission probability of fast ions is contained in the weight functions and therefore considered by the tomography. As indicated by the cross-hatched area, we do not provide information on the low energy region because of our restriction in the observable wavelength range to fast ions above 10 keV. The overall shape of the reconstructed fast-ion velocity-space distribution functions shows a maximum at positive pitch values which is well within the expectation for fast ions generated the NBI source that was operational during the experiment. However, the reconstruction suggests slightly higher fast-ion energies than expected from this 60 keV source, possibly explained by impurity radiation at large wavelength shifts that has misleadingly been identified as FIDA radiation.

Despite this uncertainty, the tomographic reconstruction allows us to provide, for the first time, a direct measurement of the redistribution level of fast ions because the impurity radiation from the plasma edge, which, most likely causes the too high energies is only weakly affected by the sawtooth crashes. By integrating the inferred velocity space distribution in energy and pitch, we find a fast-ion density before the crash of 7.4×10^{12} fast ions/cm^3 and a fast-ion density of 5.2×10^{12} fast ions/cm^3 after the sawtooth crash. This corresponds to a redistribution level of about 30% of the central fast ion population. It should be emphasised that we present here an estimate covering the entire velocity-space above 10 keV while previous studies [7, 10] reported on fast-ion densities only in specific parts of the velocity-space. In addition, the tomographic reconstruction permits us to study the pitch-angle dependence of the sawtooth-induced fast-ion redistribution. Figure 4c, illustrates the relative change of the fast-ion density at 30 keV which exhibits a strong pitch dependence. The relative crash size increases

monotonically with the pitch value. From pitch 0.0 - 0.7 the increase is modest ranging from about 15% to 25%. Then the crash size increases significantly for mainly co-rotating fast ions. Therefore, particles moving parallel to the evolving field lines are affected most by sawtooth crashes while fast ions with signficiant velocity components perpendicluar to the magnetic field are less sensitive to the sawooth instability. This result is in agreement with [7] and [8] and will be compared with MHD modeling results in future publications. Moreover, it should be noted that further improvements of the tomographic reconstruction are planned by using a fifth FIDA view, by modeling or avoiding impurity radiation and by combining the FIDA measurements with data from collective Thomson scattering [26].

3. Fast-ion current drive study

The ASDEX Upgrade tokamak is very well equipped for neutral beam current drive studies because it has sensitive set of fast-ion diagnostics, an MSE diagnostic and a flexible heating and current drive system. Eight neutral beam sources with each 2.5 MW of heating power are available of which six beams have a radial, on-axis geometry and two beams have an off-axis, tangential geometry. In addition, up to 5 MW of electron cyclotron resonance heating (ECRH) and current drive (ECCD) are available to maintain constant electron temperatures (feedback control of T_e) and to stabilize MHD instabilities [27, 28].

The NBI fast-ion current drive has been investigated in discharges where two radial on-axis NBI beams with 93 keV maximum injection energy were replaced by two tangential off-axis NBI beams (93 keV). The discharges were operated with a toroidal field of -2.6 T and a feedback controlled plasma current of 0.8 MA. Throughout the experiments, 2.5 MW of on-axis heating power was applied by the 60 keV source NBI Q3 that is needed for CXRS, MSE and FIDA measurements. Moreover, ≈ 1.5 MW of ECCD were applied to avoid sawtooth crashes (co-ECCD inside q=1) and a (2,1) magnetic island (co-ECCD at the q=2 surface). Between 4 s and 7 s, two additional 93 keV on-axis NBI sources (5 MW) were replaced by tangential off-axis NBI (also 5 MW).

The effect of this change in the NBI scheme on profiles of the electron and ion temperatures, as well as on those of the electron density and plasma rotation frequency can be seen in figure 5 for a representative discharge, #30841. The electron density remains constant while the central ion temperature and rotation drop during the off-axis NBI phase, explained by reduced central heating and momentum input. We tried

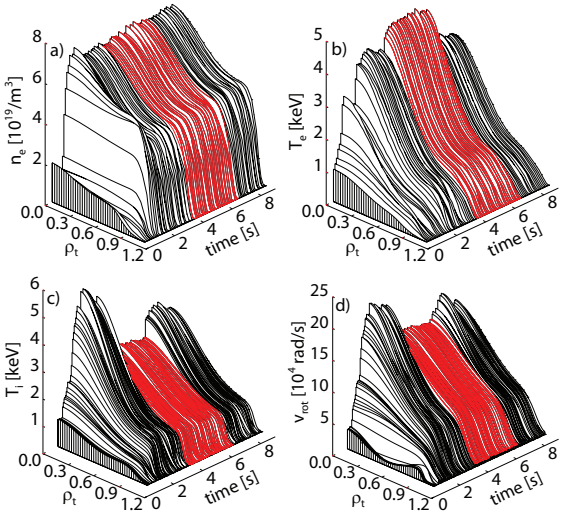

Figure 5. Bulk plasma profiles of discharge #30841 showing the electron density (a), the electron temperature (b), the ion temperature (c) and the toroidal plasma rotation frequency (d). The profiles acquired during off-axis NBI are plotted in red.

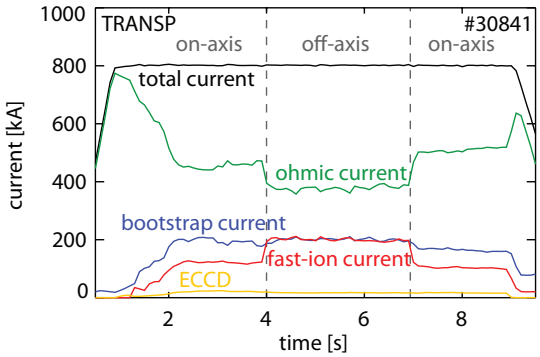

Figure 6. TRANSP predicted contributions to the total plasma current when assuming neoclassical fast-ion transport.

to keep the electron temperature profile constant during the experiment by adding $\approx$ 0.8 MW of feedback controlled central ECRH power between 4 s and 7 s because constant electron temperatures are necessary for NBI current drive studies. The shape of the ohmic current profile depends strongly on T_e and significant changes would make the analysis of the off-axis neutral beam current drive efficiency very difficult. Here, the electron temperature is slightly too high in the plasma center during the off-axis phase. This is not ideal but can be taken into account by the forward modeling.

Based on the evolution of the total plasma current, the kinetic profiles, the separatrix position and details of the heating and current drive sources, TRANSP predicts the ohmic current (resistivity by [29]), the bootstrap current (using [29]), the current driven by ECCD, and the current driven by the fast ions (using [30]). In figure

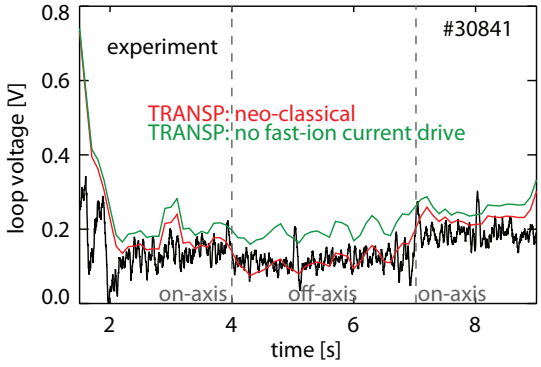

Figure 7. Measured loop voltage compared with predictions from TRANSP. The simulation plotted in red takes the current driven by the fast ions into account while the simulation given in green does not.

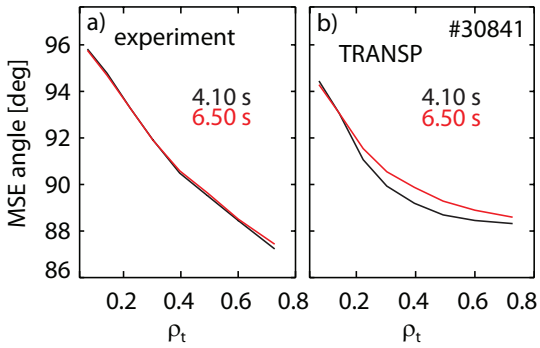

Figure 8. Measured and TRANSP-predicted (neoclassical) MSE angles for the two time points shortly after switching on off-axis NBI and after 2.5 s of off-axis NBI.

6, the predicted evolution of these components is illustrated. As expected, an increased fast-ion current (plotted in red) is predicted during the off-axis NBI phase between 4 s and 7 s which is mainly explained by the more tangential injection geometry of the off-axis beams. This increase is immediately balanced by a reduction of the feedback controlled ohmic current while the contributions of the bootstrap current and the current driven by ECCD remain constant.

Experimentally, a reduced ohmic current is observed since the loop voltage, induced by the ohmic transformer coil to drive the current, drops. As shown in figure 7, the measured loop voltage is reduced by about $\approx 50\%$ between 4 and 7 s. This observation is in agreement with the TRANSP predicted loop voltage, shown in red. In contrast, when assuming no current driven by the fast ions (simulation plotted in green), prediction and experiment disagree. This shows without ambiguity that the reduction of the loop voltage is mainly caused by an increased current-drive from the off-axis NBI.

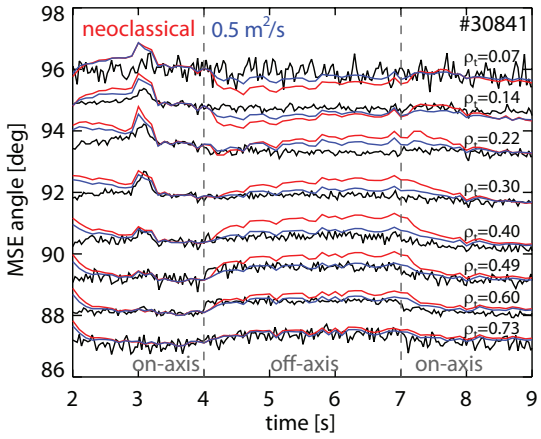

Figure 9. Temporal evolution of the measured and predicted MSE angles. In red, the neoclassical prediction by TRANSP is shown. The prediction in blue represents an anomalous fast-ion transport of $0.5\,\mathrm{m}^2/\mathrm{s}$.

In contrast to this good agreement with the neoclassical simulation, the comparison between measured and predicted current profiles shows clear differences. Figure 8 compares measured and predicted profiles of MSE angles for two time points during the off-axis phase. The MSE diagnostic measures a projection of the $\mathbf{v}_{NBI} \times \mathbf{B}$ electric field vector on the plane perpendicular to its lines of sight and is sensitive to changes in the poloidal magnetic field. The predicted MSE profile, plotted in figure 8b, shows a clear change between 4.1 s and 6.5 s (shortly and 2.5 s after switching to off-axis NBI). We expect a change during the off-axis phase because the current profile and, hence, the poloidal magnetic field, are supposed to vary slowly on the resistive time scale of seconds. The measured MSE profiles, in contrast, hardly exhibit any changes (see figure 8a).

Also when comparing the temporal evolution of the MSE data with the prediction by TRANSP, a clear disagreement is observed with the neoclassical simulation. Figure 9 shows time traces of the individual channels of the MSE diagnostic. A radial sweep of the plasma at $\approx 3\,\mathrm{s}$ proves the reliability of the diagnostic because a clear change in the measurement becomes visible which is well reproduced by TRANSP. Moreover, the diagnostic resolves well a step in the measured MSE angles at 4 s directly after the application of off-axis NBI that is explained by a change of the Shafranov shift, induced by a variation in the fast-ion pressure profile. To be able to compare the time evolution with the TRANSP prediction, a channel dependent offset has been added to the simulation to match the experimental data between 3.5 s and 4 s. As can be seen, the neoclassically predicted MSE angles in red change much more than the measured ones.

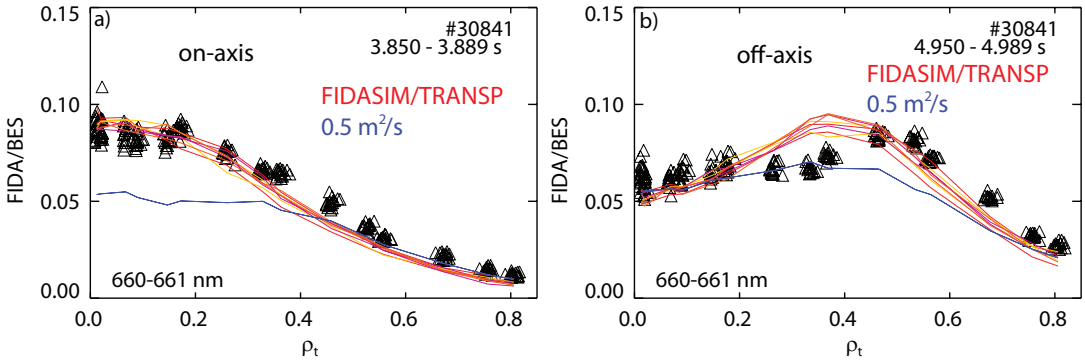

Figure 10. Radial FIDA/BES profiles during on-axis NBI (a) and off-axis NBI (b) with 2.5 ms time resolution compared with predictions by TRANSP/FIDASIM. In shades of red, a sensitivity scan of neoclassical predictions is shown that is based on the variation of the kinetic profiles input to TRANSP (plus and minus one sigma of the measurement uncertainties of T_e, T_i, n_e, Z_{eff}). In blue, TRANSP/FIDASIM predictions are illustrated that represent an anomalous fast-ion transport of $0.5\,m^2/s$

However, when assuming a global anomalous fast-ion transport of $0.5\,m^2/s$, constant in time and phase space, in the simulation, better agreement is obtained (see the blue curve in figure 9). It should be noted that assuming anomalous transport in the simulation does not significantly change the loop voltage and the total current that is driven by the fast ions. The anomalous diffusion mainly broadens the fast-ion profile. The reduced current drive efficiency of fast ions that are redistributed outwards (e.g. lost or slowed down more quickly) is balanced by an inward diffusion of fast ions. When approaching the plasma center, the slowing down time becomes longer and the redistributed fast particles can contribute more to the plasma current.

The possibility of anomalous fast-ion transport has been checked by analyzing radial profiles of co-rotating fast ions using the FIDA diagnostic. In figure 10, radial profiles of the FIDA/BES ratio are compared with TRANSP/FIDASIM predictions. Passive radiation, measured during phases without operation of the diagnostic NBI, has been subtracted from the signal. The measurements, as well as the predictions from TRANSP, show a clear change of the FIDA/BES profiles when switching from on-axis NBI to off-axis NBI. In order to make a sensitivity scan of the prediction, 8 synthetic profiles have been calculated by TRANSP and FIDASIM with input kinetic profiles (T_e, T_i, n_e, Z_{eff}) that represent the statistical measurement uncertainties ($\pm$ one standard deviation). As can be seen, the measurement during on-axis NBI (figure 10a) agrees well with the scan of neoclassical simulations potted in red shades. In contrast, a simulation assuming a global fast-ion transport of $0.5\,m^2/s$ does not represent the

measurement. During off-axis NBI, the measured profiles are slightly flatter than the neoclassical predictions. In particular between $\rho_t = 0.2$ and $\rho_t = 0.4$, the measured profiles agree better with the assumption of anomalous fast-ion transport. The origin of this additional transport mechanism might be explained by the presence of small scale turbulence or by the mode activity visible in the magnetic measurements. Despite attempts to perform MHD quiescent experiments, n=1, m=1 modes in the frequency range between 10 kHz and 25 kHz at $\rho_t \approx 0.25$ could not be avoided. These modes might change the current distribution and the fast-ion profiles and must be avoided in future experiments, possibly by performing experiments with the q_{min} above one.

4. Summary and conclusion

The fast-ion measurements at ASDEX Upgrade permit detailed investigation of the fast-ion transport properties. During sawtooth crashes, very strong fast-ion redistribution is measured by an array of toroidal FIDA views that is in good agreement with the Kadomtsev model. 2D fast-ion velocity distribution functions in the plasma center have been calculated based on 4-view FIDA measurements which are easier to interpret than the raw FIDA spectra. They show a clear drop of the central fast-ion density after sawtooth crashes and a stronger redistribution of purely passing fast ions than of those ions with pitch values in the vicinity of zero.

In NBI current drive experiments, the loop-voltage changes in agreement with the neoclassical prediction when replacing on-axis NBI by off-axis NBI. However, measurements of the MSE diagnostic do not agree with the predictions by TRANSP. Instead, when assuming a global anomalous fast-ion transport, the MSE measurement can be explained better. This transport is also needed when comparing modeled profiles from the FIDA diagnostic with the experimental data. The measurements during off-axis NBI are slightly flatter than the neoclassical predictions from TRANSP while the application of a global anomalous fast-ion transport explains certain properties of the measurement. However, a more sophisticated physics based model is needed to better describe the measurement and is subject to future work. For this purpose, the source of the anomalous fast-ion transport must be identified which could be caused by (1,1) MHD activity or turbulence. New experiments without (1,1) MHD activity are consequently planned in the 2015 experimental campaign.

5. Acknowledgements

This work has been carried out within the framework of the EUROfusion Consortium and has received funding from the Euratom research and training programme 2014-2018 under grant agreement No 633053. The views and opinions expressed herein do not necessarily reflect those of the European Commission.

[1] FISCH, N. J., Rev. Mod. Phys. **59** (1987) 175.
[2] GARCA-MUOZ, M. et al., Nuclear Fusion **49** (2009) 085014.
[3] VON GOELER, S. et al., Phys. Rev. Lett. **33** (1974) 1201.
[4] IGOCHINE, V. et al., Nuclear Fusion **47** (2007) 23.
[5] MARCUS, F. B. et al., Plasma Physics and Controlled Fusion **33** (1991) 277.
[6] LOVBERG, J. A. et al., Physics of Fluids B: Plasma Physics **1** (1989) 874.
[7] MUSCATELLO, C. M. et al., Plasma Physics and Controlled Fusion **54** (2012) 025006.
[8] NIELSEN, S. K. et al., Plasma Physics and Controlled Fusion **52** (2010) 092001.
[9] CECCONELLO, M. et al., Plasma Physics and Controlled Fusion **57** (2015) 014006.
[10] GEIGER, B. et al., Nuclear Fusion **54** (2014) 022005.
[11] GUENTER, S. et al., Nuclear Fusion **47** (2007) 920.
[12] TURNYANSKIY, M. et al., Nuclear Fusion **49** (2009) 065002.
[13] PACE, D. C. et al., Physics of Plasmas **20** (2013) 056108.
[14] GEIGER, B. et al., Plasma Physics and Controlled Fusion **57** (2015) 014018.
[15] HEIDBRINK, W. W. et al., Plasma Physics and Controlled Fusion **46** (2004) 1855.
[16] A HERRMANN, O. G. et al., Fusion Science and Technology **44** (2003) 569.
[17] TARDINI, G. et al., Journal of Instrumentation **7** (2012) C03004.
[18] PANKIN, A. et al., Computer Physics Communications **159** (2004) 157 .
[19] PORCELLI, F. et al., Plasma Physics and Controlled Fusion **38** (1996) 2163.
[20] GEIGER, B. et al., Review of Scientific Instruments **84** (2013) .
[21] HEIDBRINK, W. et al., Commun. Comput. Phys. **10** (2011) 716.
[22] SALEWSKI, M. et al., Nuclear Fusion **52** (2012) 103008.
[23] SALEWSKI, M. et al., Nuclear Fusion **53** (2013) 063019.
[24] SALEWSKI, M. et al., Nuclear Fusion **54** (2014) 023005.
[25] SALEWSKI, M. et al., Plasma Physics and Controlled Fusion **56** (2014) 105005.
[26] MEO, F. et al., Journal of Physics: Conference Series **227** (2010) 012010.
[27] ZOHM, H. et al., Nuclear Fusion **41** (2001) 197.
[28] MÜCK, A. et al., Plasma Physics and Controlled Fusion **47** (2005) 1633.
[29] SAUTER, O. et al., Physics of Plasmas (1994-present) **6** (1999).
[30] LIN-LIU, Y. R. et al., Physics of Plasmas (1994-present) **4** (1997).